Title: Thermally Induced Oxidation of [FeII(tacn)2](OTf)2 (tacn = 1,4,7-triazacyclononane)

Authors: Jia Li; Atanu Banerjee; Debra Preston; Brian Shay; Amitiva Adhikary; Michael Sevilla; Reza Loloee; Richard Staples; Ferman Chavez

To be cited as: 10.1002/ejic.201701190

Link to VoR: https://doi.org/10.1002/ejic.201701190

Thermally Induced Oxidation of $[Fe^{II}(tacn)_2](OTf)_2$ (tacn = 1,4,7-triazacyclononane)

Jia Li,[a] Atanu Banerjee, [a] Debra R. Preston,[a] Brian J. Shay,[b] Amitiva Adhikary,[a] Michael D. Sevilla,[a] Reza Loloee,[c] Richard J. Staples,[d] and Ferman A. Chavez*[a]

.

[a] Department of Chemistry, Oakland University, Rochester, MI 48309-4477, USA
[b] Biomedical Mass Spectrometry Facility, University of Michigan, Ann Arbor, MI 48109-0632, USA
[c] Department of Physics and Astronomy, Michigan State University, East Lansing, MI 48824-1322, USA
[d] Department of Chemistry, Michigan State University, East Lansing, MI 48824-1044, USA

Abstract

We previously reported the spin-crossover (SC) properties of $[Fe^{II}(tacn)_2](OTf)_2$ (**1**) (tacn = 1,4,7-triazacyclononane) [*Eur. J. Inorg. Chem.* **2013**, 2115]. Upon heating under dynamic vacuum, **1** undergoes oxidation to generate a low spin iron(III) complex. The oxidation of the iron center was found to be facilitated by initial oxidation of the ligand via loss of an H atom. The resulting complex was hypothesized to have the formulation $[Fe^{III}(tacn)(tacn\text{-}H)](OTf)_2$ (**2**) where tacn-H is *N*-deprotonated tacn. The formulation was confirmed by ESI-MS. The powder EPR spectrum of the oxidized product at 77 K reveals the formation of a low-spin iron(III) species with rhombic spectrum (g = 1.98, 2.10, 2.19). We have indirectly detected H_2 formation during the heating of **1** by reacting the headspace with HgO. Formation of water (^{1}HNMR in anhydrous d_6-DMSO) and elemental mercury were observed. To further support this claim, we independently synthesized $[Fe^{III}(tacn)_2](OTf)_3$ (**3**) and treated it with one equiv base yielding **2**. The structures of **3** was characterized by X-ray crystallography. Compound **2** also exhibits a low spin iron(III) rhombic signal (g = 1.97, 2.11, 2.23) in DMF at 77 K. Variable temperature magnetic susceptibility measurements indicate that **3** undergoes gradual spin increase from 2 to 400 K. DFT studies indicate that the deprotonated nitrogen in **2** forms a bond to iron(III) exhibiting double bond character (Fe-N, 1.807 Å).

Introduction

Hydrogen atom transfer (HAT) reactions are those wherein both a proton and electron are transferred.[1] Such a mechanism avoids the generation of high energy intermediates.[2] HAT reactions may also be viewed as a more general proton-coupled electron transfer (PCET).[3] These reactions have been increasingly observed in reactions catalyzed by metalloenzymes.[1b, 4] Examples of PCET in biological systems include lipoxygenases,[5] oxalate decarboxylase,[6] photosystem II,[7] cytochrome *c* oxidase,[8] cytochrome P450,[9] methane monooxygenases,[10] and ribonucleotide reductases.[11] Previous studies using $[Fe^{II}(H_2bip)]^{2+}$ and $[Fe^{II}(H_2bim)]^{2+}$ (H_2bip = 2,2′-bi(tetrahydropyrimidine; H_2bim = 2,2′-bi-2-imidazoline) and TEMPO (Eq. 1 and 2), have demonstrated this type of reaction in iron-containing model complexes.[1a, 1f, 4a, 12]

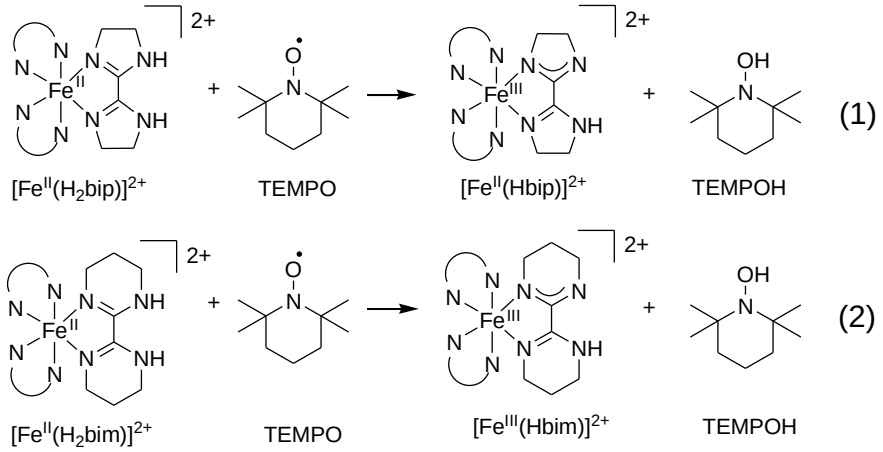

In this work we report a PCET reaction which takes place upon heating of $[Fe^{II}(tacn)_2](OTf)_2$ (**1**) (tacn = 1,4,7-triazacyclononane)[13] under dynamic vacuum. The loss of an H atom from the complex results in formal oxidation of the iron(II) center to iron(III) and the generation of $[Fe^{III}(tacn)(tacn\text{-}H)]^{2+}$ (**2**) where tacn-H = *N*-deprotonated tacn. We discuss the spectroscopic properties of **2** along with the synthesis and characterization of $[Fe^{III}(tacn)_2](OTf)_3$

(**3**) and subsequent conversion of **3** to **2** via reaction with base. Theoretical (DFT) studies for **3** and **2** are also presented.

Results and discussion

Our laboratory previously reported the non-ideal spin crossover behavior for $[Fe^{II}(tacn)_2](OTf)_2$ (**1**).[13] We subsequently discovered the reason for this behavior. Heating $[Fe^{II}(tacn)_2](OTf)_2$ in the solid state under dynamic vacuum results in oxidation of the iron(II) center to iron(III). The temperature-dependent magnetic susceptibility can be seen to change when powdered $[Fe^{II}(tacn)_2](OTf)_2$ sample is heated at 400 K for 24 h (Figure 1, closed circles). The increase in magnetic susceptibility at 2 K ($\chi_M T$ = 0.4 cm^3 mol^{-1} K) is consistent with the quantitative formation of iron(III) which would have one unpaired spin (S = 1/2) in the low spin case compared to iron(II) (S = 0). When the sample is heated to 400 K, there is a slight increase in $\chi_M T$ value up to 300 K with a larger change after that suggesting moderate spin crossover behavior.

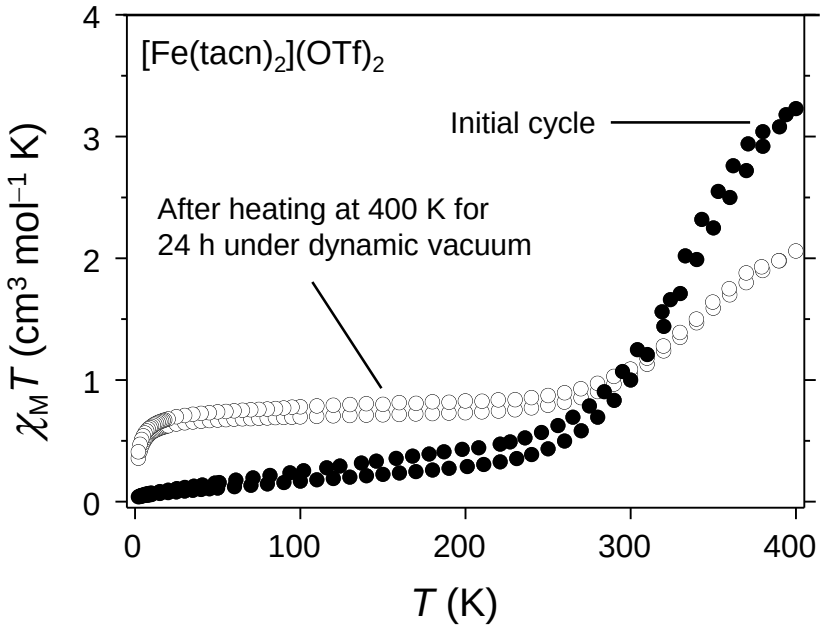

Figure 1. Heat-induced oxidation of $[Fe^{II}(tacn)_2](OTf)_2$ (**1**) in the SQUID magnetometer at 0.1 T.

X-band EPR studies (Figure 2) on solid samples of $[Fe^{II}(tacn)_2](OTf)_2$ under nitrogen initially reveal an EPR-silent species. Upon sample grinding and heating to 400 K for 6 h under dynamic vacuum, a signal (12%) is observed in the $g \sim 2$ region corresponding to a low spin rhombic iron(III) signal (g = 1.98, 2.10, 2.19). A small amount of high spin iron(III) signal ($g \sim$ 4.3) first observed at 6 h (0.2%). When the sample is heated for an additional 6 h, the low spin rhombic iron(III) signal becomes larger (20%) and more symmetrical. The high spin iron(III) signal also increases slightly (0.5%). After a total of 24 h of heating under dynamic vacuum the $g \sim 2$ region becomes larger and changes noticeably exhibiting a new rhombic signal (g = 1.98, 2.14, 2.38). The high spin iron(III) signal also becomes larger (22%). The presence of broad signals near g ~ 2 and the g ~ 4.3 signal indicates some decomposition has occurred. Importantly, no oxidation is observed when the sample is heated to 400 K under static vacuum (headspace = 50 mL) even after 3 d.

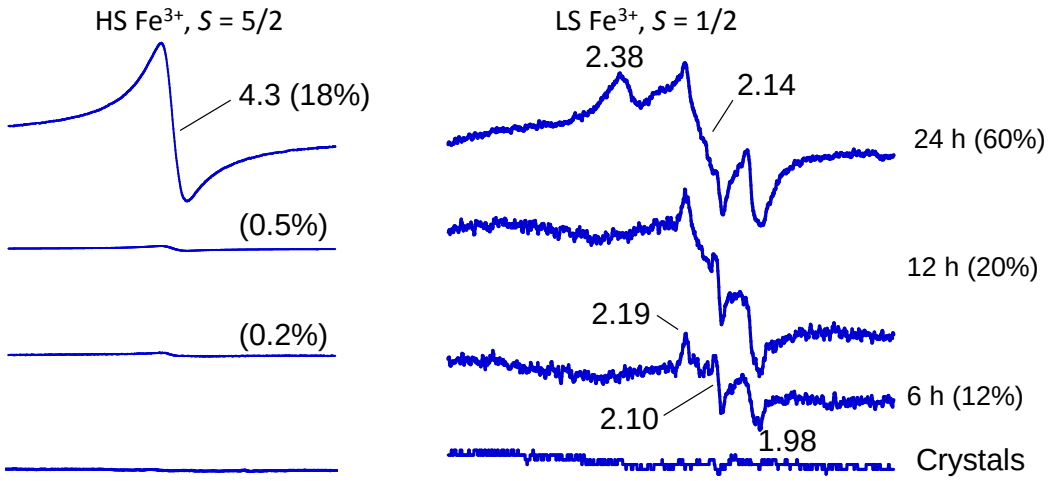

Figure 2. X-band EPR spectrum (77 K) of solid $[Fe^{II}(tacn)_2](OTf)_2$ (**1**) heated (400 K) under dynamic vacuum. Selected g values are indicated. Spectrometer settings: microwave frequency 9.43 GHz; microwave power, 0.22 mW; modulation frequency, 100 kHz; modulation amplitude, 8 G; gain, 1 x 10^4. Note that the g ~ 2 spectrum for the 24 h sample was scaled by one half.

To probe the products formed during this oxidation process, mass spectrometry was employed. Solid samples of $[Fe^{II}(tacn)_2](OTf)_2$ were heated to 400 K under dynamic vacuum for 6 h and the resulting solid was dissolved in DMF which was then analyzed by electrospray ionization mass spectrometry (ESI-MS) (Figure 3).

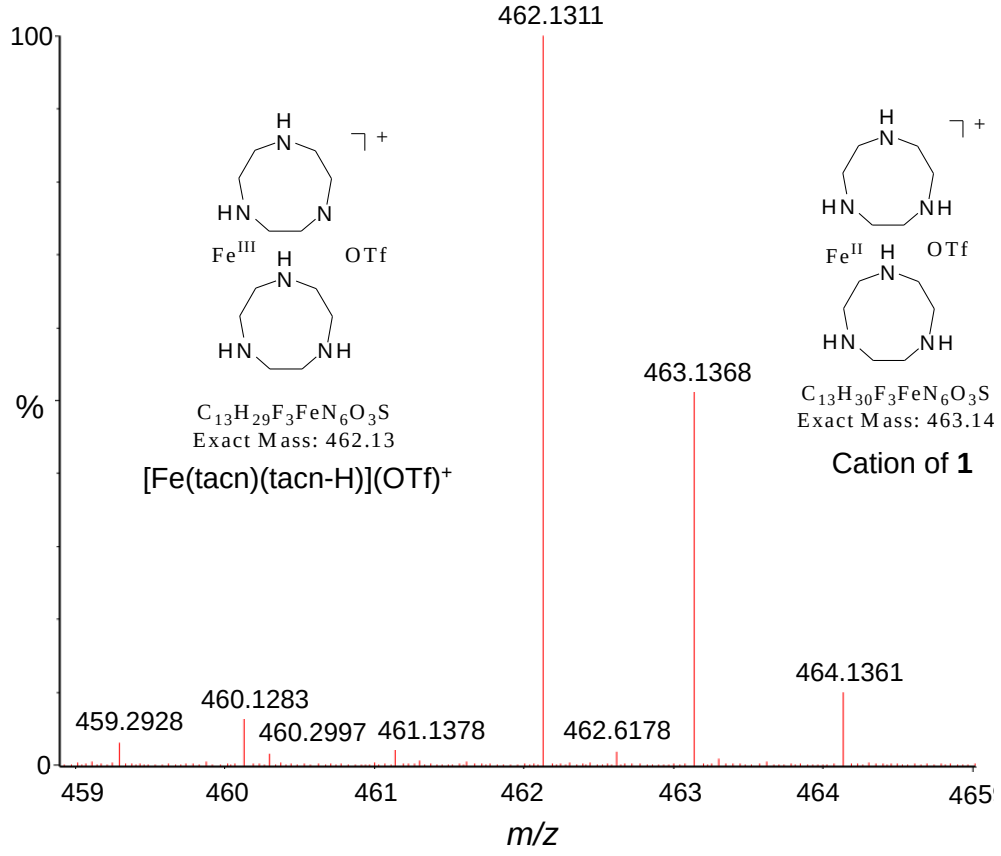

Figure 3. Positive ESI mass spectrum of $[Fe^{II}(tacn)_2](OTf)_2$ (**1**) after being heated in the solid state to 400 K under vacuum for 6 h. Solvent: DMF.

The samples were found to exhibits $[Fe^{II}(tacn)_2](OTf)^+$ (*m/z* = 463.14) and $[Fe^{III}(tacn)(tacn\text{-}H)](OTf)^+$ (*m/z* = 462.13) (where tacn-H = *N*-deprotonated tacn). These results indicate that when $[Fe^{II}(tacn)_2](OTf)_2$ is heated under dynamic vacuum, H atoms are lost

possibly combining to form H_2 (Eq. 3). We hypothesize that within the crystal lattice, heating results in the release of an H atom which subsequently abstracts an H atom from an adjacent iron(II) complex (facilitating oxidation).

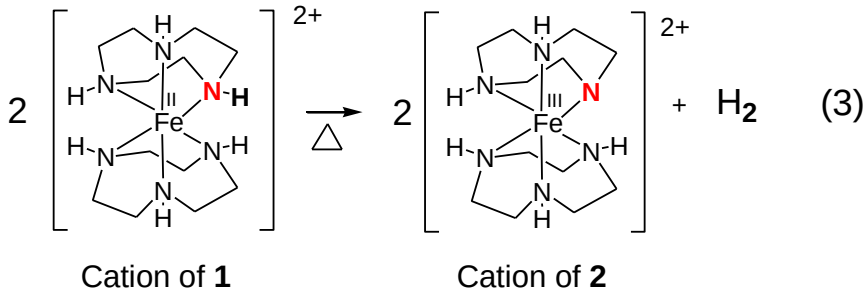

Cation of **1** Cation of **2**

To test this hypothesis, we devised an experiment to detect H_2 in the headspace of the reaction. Mercury(II) oxide (HgO) is known to react with hydrogen irreversibly to generate elemental mercury and water.[14] If the reaction headspace contains H_2 we should observe the formation of these two products when it is heated in the presence of HgO. To trap any headspace gas generated during heating we attached a 50 mL flask containing HgO immersed in liquid nitrogen to the reaction flask separated by a stopcock. After heating the reaction flask containing 500 mg of **1** for 3 d under static vacuum at 400 K, we closed the stopcock and heated the 50 mL to 265°C for 24 h. Two control experiments were also conducted under the same conditions. The negative control lacked compound **1** while to the positive control was added 50 mL of dry H_2 gas. After heating the flasks were then cooled to 25°C and taken into a glovebox. To the flasks was added 1.0 mL of anhydrous d_6-DMSO. The flasks were then stoppered and shaken. The results of this experiment are shown in Figure 4. The results clearly indicate the formation of water which is consistent with the formation of hydrogen gas during the heating of **1** under

vacuum. A mercury film was also observed for the sample and positive control (faint in the case of the sample experiment) but not for the negative control.

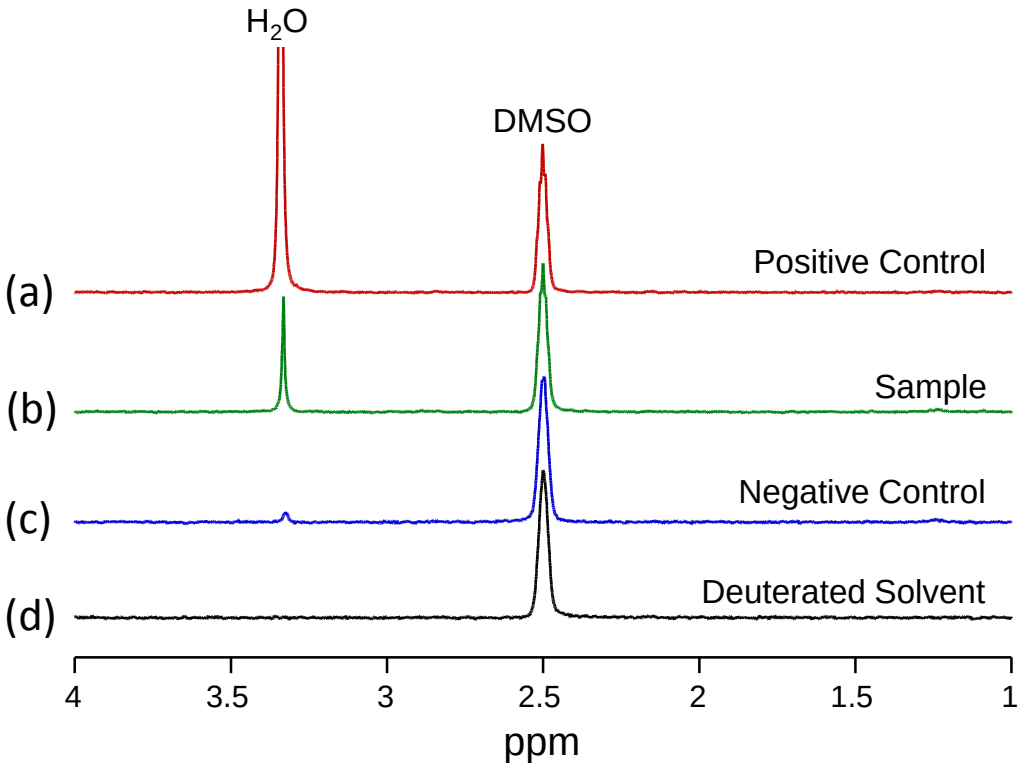

Figure 4. ^{1}HNMR spectra (25 ºC) of (a) positive control (H_2 was heated in the presence of HgO in a closed vessel and then extracted with 1 mL of d_6-DMSO), (b) sample (headspace gas generated from heating $[Fe^{II}(tacn)_2](OTf)_2$ (**1**) under vacuum was heated in the presence of HgO in a closed vessel and then extracted with 1 mL of d_6-DMSO), (c) negative control (same experiment as in (b) in the absence of **1**), (d) d_6-DMSO used in the experiments.

In our attempts to independently synthesize $[Fe^{III}(tacn)(tacn\text{-}H)](OTf)_2$ (**2**) for characterization and to compare its properties with the thermally-induced oxidation product of **1**, we first synthesized the iron(III) analogue $[Fe^{III}(tacn)_2](OTf)_3$ (**3**) with the goal of deprotonating it to generate **2**.

To synthesize **3** we first prepared an iron(III) starting material ($[Fe^{III}(DMF)_6](OTf)_3$). This compound had not been previously reported but was found to have advantages over using commercially available $Fe(OTf)_3$ as the iron source. First, it has a larger molar mass (making it easier to weigh out) and second, it can be isolated in high purity crystalline form (unlike commercially available $Fe(OTf)_3$ which is typically contains 10% impurity). Compound **3** was synthesized by reacting $[Fe^{III}(DMF)_6](OTf)_3$ with two equiv tacn in methanol. Diffusion of ether afforded bright orange crystals of **3** in good yield. UV-vis spectroscopy measurements in methanol and acetonitrile yielded similar spectra with peaks near 335 nm (400 M^{-1} cm^{-1}), 430 nm (100 M^{-1} cm^{-1}), and 513 nm (50 M^{-1} cm^{-1}). These bands are consistent with those observed for other iron(III) complexes.[15]

X-ray Crystallography

The X-ray structure of **3** was determined. The crystallographic parameters for **3** are given in Table 1 while Table 2 contains bond distances and angles. The structure of **3** is shown in Figure 5. The iron(III) center is coordinated by two tacn ligands in a tridentate fashion and possesses distorted octahedral geometry. Fe-N bond distances were found to range between 1.99–2.00 Å which is consistent with other iron(III) compounds rich in nitrogen coordination.[16] These bond distances are only slightly shorter compared to the iron(II) analogue while the *trans* N-Fe-N bond angles are quite similar.[13] The structure also revealed a substantial H-bonding network involving the N-H groups and the triflate groups. Methanols are also involved in this bonding network (Figure 5).

Table 1. Crystallographic data and refinement results for $[Fe^{III}(tacn)_2](OTf)_3$ (**3**).

Formula	$C_{19}H_{43}F_9FeN_6O_{12}S_3$
fw/gmol^{-1}	870.62
Temperature/K	173.15
Crystal system	monoclinic
Space group	$P2_1/n$
a/Å	9.0622(6)
b/Å	28.8446(19)
c/Å	13.6738(9)
α/Å	90
β/Å	94.5010(10)
γ/Å	90
Volume/A^3	3563.2(4)
Z	4
ρ_{calc}/Mgm^{-3}	1.623
GOF	1.054
Final R indices [$I>2\sigma(I)$]	$R1$=0.0611, $wR2$=0.1505

Table 2. Selected bond distances and angles of $[Fe^{III}(tacn)_2](OTf)_3$ (**3**). Calculated values are shown in brackets.

Bond Lengths (Å)			
Fe-N(1)	2.00(3) [2.02]	Fe-N(4)	2.00(3) [2.02]
Fe-N(2)	2.00(3) [2.02]	Fe-N(5)	1.99(3) [2.01]
Fe-N(3)	1.99(3) [2.01]	Fe-N(6)	2.00(3) [2.02]
Bond Angles (º)			
N(1)-Fe-N(2)	84.3(13) [84.3]	N(5)-Fe-N(2)	92.5(13) [96.2]
N(1)-Fe-N(4)	93.6(14) [94.9]	N(5)-Fe-N(3)	175.3(13) [179.2]
N(3)-Fe-N(1)	84.9(13) [83.0]	N(5)-Fe-N(4)	84.7(13) [83.0]
N(3)-Fe-N(2)	84.4(13) [83.3]	N(5)-Fe-N(6)	85.2(13) [83.3]
N(3)-Fe-N(4)	98.5(13) [97.5]	N(6)-Fe-N(1)	175.4(14) [178.8]
N(3)-Fe-N(6)	91.8(13) [96.2]	N(6)-Fe-N(2)	98.5(14) [96.5]
N(4)-Fe-N(2)	176.2(14) [178.8]	N(6)-Fe-N(4)	83.8(14) [84.3]
N(5)-Fe-N(1)	98.3(13) [97.5]		

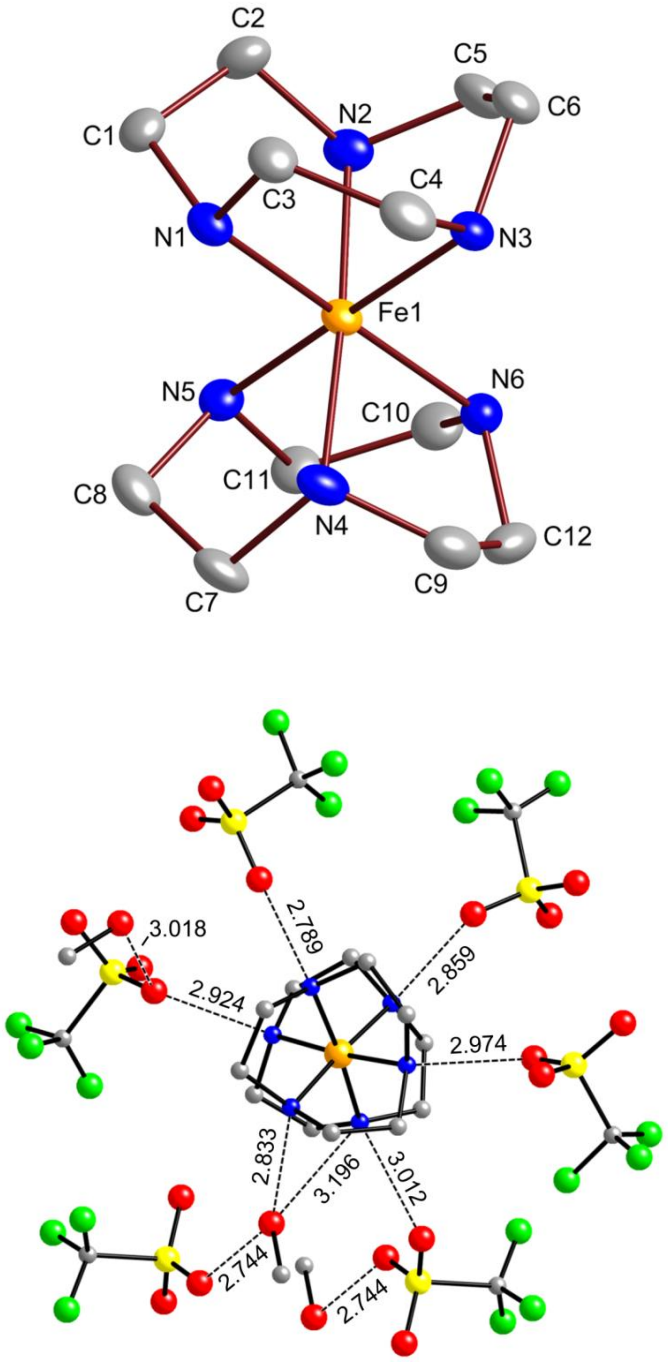

Figure 5. (Top) X-ray structure (50% thermal ellipsoids) of $[Fe^{III}(tacn)_2](OTf)_3$ (**3**) with H atoms omitted for clarity. The H-bonding network (broken lines) is also shown.

*Synthesis and characterization of [Fe^{III}(tacn)(tacn-H)](OTf)$_2$ (**2**)*

Under dry nitrogen **3** was reacted with one equiv base (NaH) in DMF (Eq. 4). Compound **2** in DMF clearly displayed a rhombic (g = 1.97, 2.11, 2.23) low spin Fe(III) signal (Figure 6) confirming that the +3 oxidation state remained after deprotonation. In Wieghardt's work, reaction of base with ([Fe^{III}(tacn)$_2$](ClO$_4$)$_3$) was found to afford the *N*-deprotonated analogue in aqueous media as well.[17]

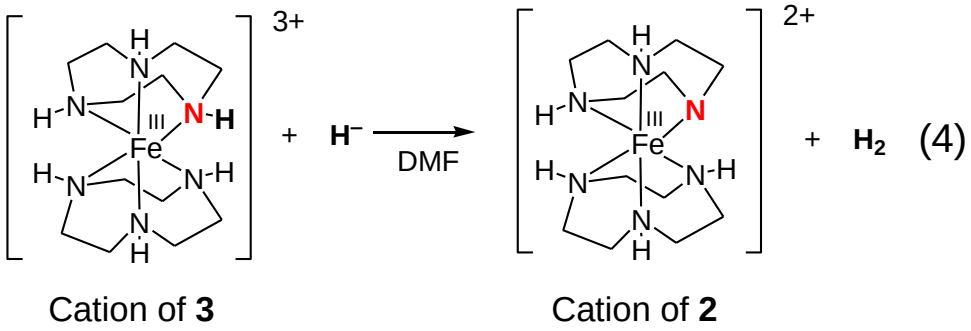

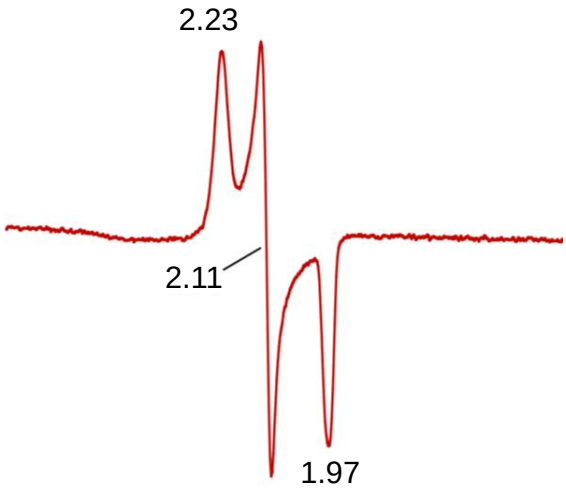

Figure 6. X-band EPR spectrum (77 K) of **2** generated by deprotonation of **3** in DMF. Selected g values are indicated. Spectrometer settings: microwave frequency 9.43 GHz; microwave power, 0.22 mW; modulation frequency, 100 kHz; modulation amplitude, 8 G; gain, 1 x 10^4.

Magnetic Measurements

Variable temperature SQUID measurements were performed on **3** and show a temperature-dependent magnetization (Figure 7). At 2 K, $\chi_M T$ has a value of 0.46 cm^3 mol^{-1} K (H = 0.1 T) which is close to the spin-only theoretical value of 0.38 cm^3 mol^{-1} K for LS Fe(III) (S = 1/2). As the temperature increases to 400 K, the value becomes ~ 0.73 cm^3 mol^{-1} K which corresponds to 1.6 unpaired electrons. The Evan's NMR method[18] for solution magnetic susceptibility was performed on **3** at 298 K and the $\chi_M T$ values of 0.6 cm^3 mol^{-1} K (MeCN) and 0.7 cm^3 mol^{-1} K (MeOH) were determined. These values are in line with the solid state value at 300 K ($\chi_M T$ = 0.66 cm^3 mol^{-1} K). Previously Wieghardt and coworkers prepared $[Fe^{III}(tacn)_2]Cl_3 \cdot 5H_2O$[16h] and $[Fe^{III}(tacn)_2]Br_3 \cdot 5H_2O$.[15] $[Fe^{III}(tacn)_2]Br_3 \cdot 5H_2O$ possesses $\chi_M T$ = 0.66 cm^3 mol^{-1} K at 20 ºC suggesting a LS state, however, to date no solid-state variable temperature magnetic data has been reported for either compound.

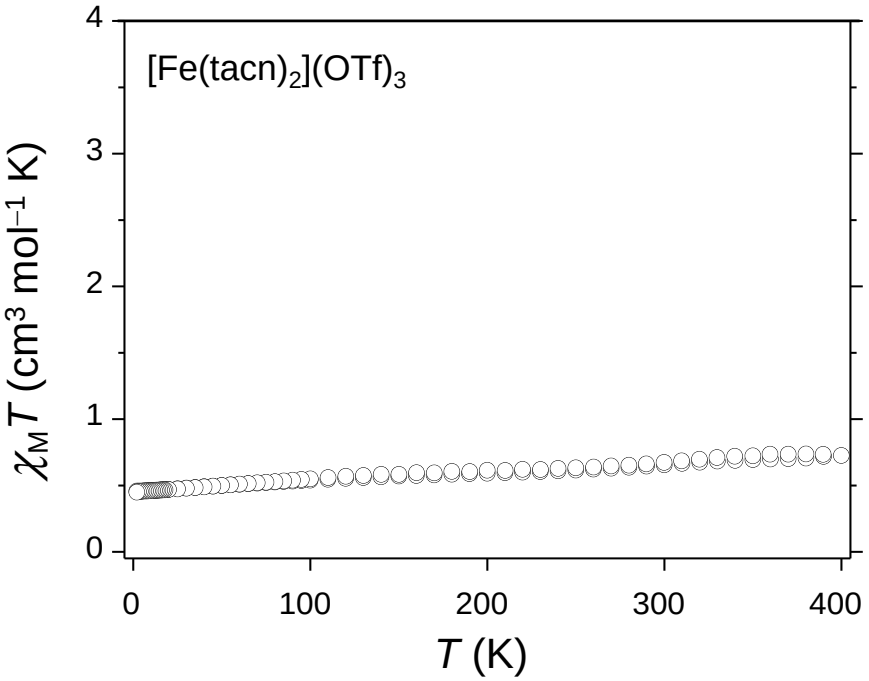

Figure 7. Temperature dependence of $\chi_M T$ (H = 0.1 T) for $[Fe^{III}(tacn)_2](OTf)_3$ (**3**).

Theoretical Calculations

DFT unrestricted calculations were carried out on complexes **2** and **3**. Ground state geometries were fully optimized in the absence of solvent. Orbital energies were calculated using PBE0/6-31G(d). A comparison between the experimental and theoretical bond distances and angles (Table 2) for **3** showed close agreement. The greatest difference between the experimental and calculated Fe-N bond lengths are 0.02 Å for **3**, respectively. The experimental and calculated N-Fe-N bond angles are also in good agreement. Given the close agreement, the calculated values represent good approximations and therefore the electronic properties for **3** can be confidently inferred. Furthermore, we can deduce high confidence in the calculated values for **2**. Figures 8 and 9 show the following molecular orbitals: HOMO, HOMO−1, LUMO, and LUMO+1 for complexes **3** and **2**, respectively.

For **3** (Figure 8) it is seen that the highest occupied molecular orbital (HOMO, β-83) is largely distributed over the Fe d_{xz}/d_{yz} orbital. HOMO−1 (β-82) is also comprised of Fe d_{xz}/d_{yz}. The energies for HOMO and HOMO−1 are very close indicating near degeneracy in the optimized structure. The lowest unoccupied molecular orbital (LUMO, β-84) is primarily distributed over the Fe d_{z^2} oribtal with very little contribution from the ligands. The metal $d_{x^2-y^2}$ orbital are associated with LUMO+1 (α-85) along with nitrogen *p* orbitals in an anti-bonding fashion. For complex **2** (Figure 9), the HOMO (α-84) is an antibonding combination between the Fe d_{xz}/d_{yz} and the N unhybridized *p* orbital. The HOMO−1 (β-83), on the other hand is a π bonding molecular orbital signifying double bond character (Fe=N) between the iron and nitrogen. This bond is also significantly shorter (1.807 Å) compared to the Fe-N bonds in Table 2 and the remaining Fe-N bonds in **2** (Average: 2.03 Å).

The LUMO (β-84) is an antibonding combination between the Fe d_{xz}/d_{yz} and the N unhybridized *p* orbital. LUMO+1 (α-85) is mainly comprised of the Fe $d_{x^2-y^2}$ oribtal in an antibonding configuration with N *p* orbitals.

The HOMO-LUMO gap for **3** (5.49 eV) is slightly larger than the same value for **2** (4.22 eV), however the absolute orbital energies for **3** (HOMO: −18.61 eV) are significantly lower compared to **2** (HOMO: −12.57 eV) consistent with the greater stability of **3**. Although the charge and spin density on the iron center in **3** (charge = +1.079) is slightly lower compared to **2** (charge = +1.125), the overall charge for **3** is greater than **2** consistent with higher stability for **3**.

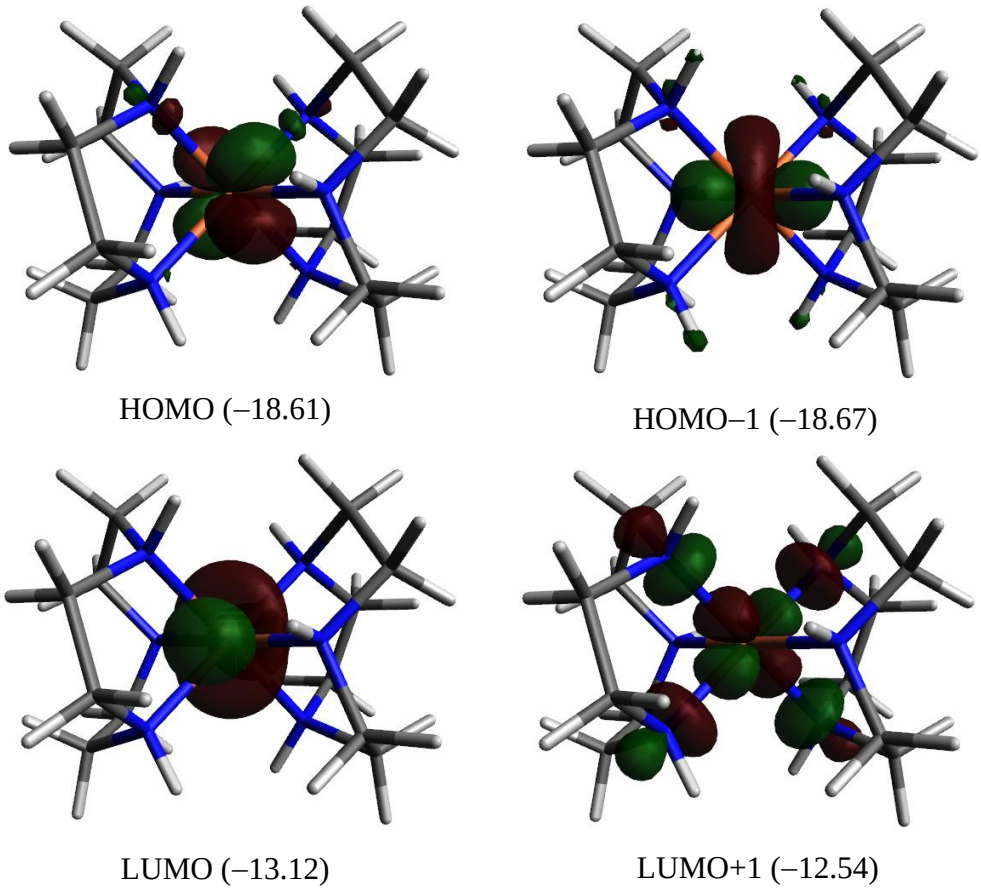

Figure 8. Plots of molecular orbitals: HOMO−1, HOMO, LUMO, and LUMO+1 for $[Fe^{III}(tacn)_2]^{3+}$ (cation of **3**). Orbital energies (eV) are indicated.

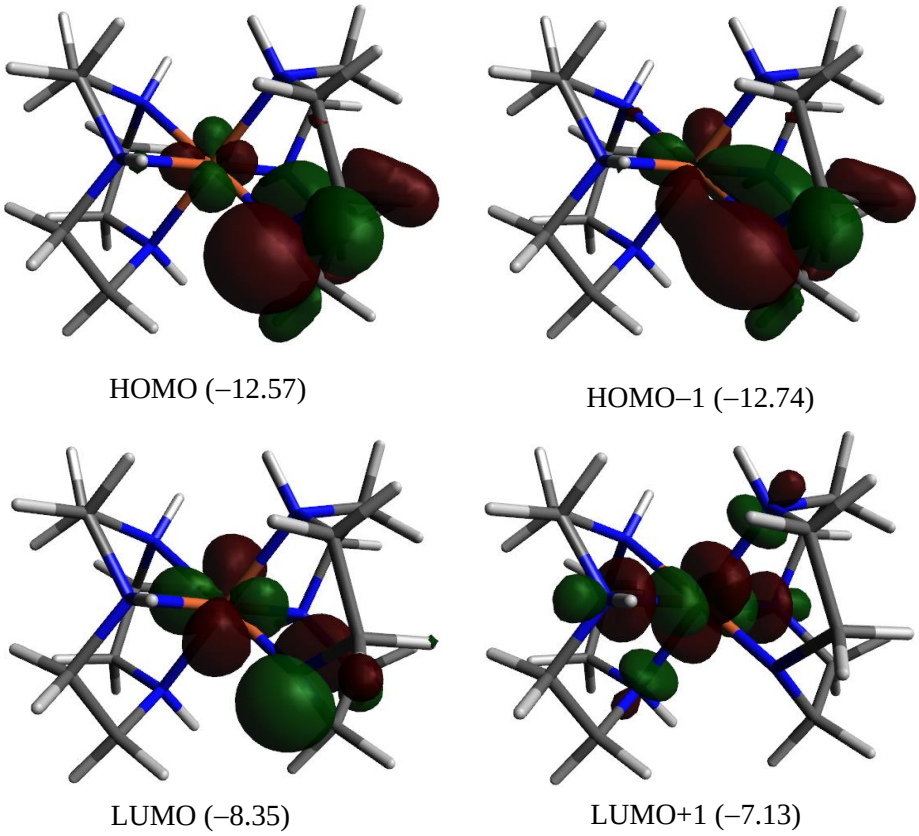

Figure 9. Plots of molecular orbitals: HOMO−1, HOMO, LUMO, and LUMO+1 for $[Fe^{III}(tacn)(tacn\text{-}H)]^{2+}$ (cation of **2**). Orbital energies (eV) are indicated.

Conclusions

In conclusion, heating $[Fe^{II}(tacn)_2](OTf)_2$ (**1**) in the solid state under dynamic vacuum results in oxidation of the iron(II) center to iron(III). This result has been confirmed by SQUID magnetic magnetometry, EPR, and ESI-MS. Oxidation of the iron center results from removal of an H atom from the ligand (coupling with another H atom to form H_2) generating a deprotonated amido nitrogen bonded to iron(III). The formulation of this product is $[Fe^{III}(tacn)(tacn\text{-}H)](OTf)_2$ (**2**, tacn-H = monodeprotonated tacn). EPR revealed that the complex contained low spin iron(III). In our efforts to independently synthesize **2**, we first prepared $[Fe^{III}(tacn)_2](OTf)_3$ (**3**)

which was structurally characterized. We then reacted **3** with NaH in DMF. This resulted in formation of the deprotonated complex **2**. Variable temperature magnetic susceptibility measurements on **3** between 2–400 K indicate that **3** undergoes a gradual increase in spin. Theoretical studies indicate that the deprotonated nitrogen in **2** forms a double bond with the iron center (Fe^{III}=N) and that complex **3** is more stable compared to **2**. The reactivity of **2** towards protic substrates will be investigated in future studies.

Experimental

General Considerations. Compound **1** was prepared as previously described.[13] Pure dry solvents (acetonitrile, DMF, ether, and dichloromethane) were obtained using an Innovative Technologies Inc. Solvent Purification System. Acetonitrile was further passed through activated alumina immediately prior to use. Methanol was distilled from magnesium methoxide under a nitrogen atmosphere and stored over 3A molecular sieves. All air sensitive manipulations were performed using standard Schlenk techniques or in a nitrogen-filled glovebox. The ligand tacn was synthesized using a literature method.[19] Elemental Analysis was performed on pulverized crystalline samples heated (40 °C) under vacuum and sealed in a glass ampule prior to submission to Atlantic Microlabs, Inc., Norcross, GA.

Synthesis

$[Fe^{III}(DMF)_6](OTf)_3$. Under nitrogen, 555.5 mg $FeCl_3$ (3.45 mmol) was dissolved in 2 mL CH_3CN and 4 mL CH_2Cl_2 and stirred. 2.556 g Me_3SiOTf (11.5 mmol) was added to the stirring solution dropwise. The solution turned deep red and was stirred overnight. The next day the solution was placed under high vacuum and the volume was reduced to 5 mL. The solution was then filtered and 1 mL DMF was added (Note: This reaction is highly exothermic). The solution

became yellow-green in color. 10 mL of ether was added and the solution was placed in the freezer. Large yellow-green crystals were deposited overnight. These crystals were collected, washed with ether and dried under vacuum. Yield: 2.65 g (79.6%). Anal. Calcd for $C_{21}H_{42}F_9FeN_6O_{15}S_3$: C, 26.79; H, 4.50; N, 8.93. Found: C, 27.24; H, 4.43; N, 9.35.

$[Fe^{III}(tacn)_2](OTf)_3$ (3). In a nitrogen-filled glovebox, 100 mg tacn (0.410 mmol) was dissolved in 1 mL MeOH. 364.9 mg $[Fe^{III}(DMF)_6](OTf)_3$ (0.20 mmol) was dissolved in 2 mL MeOH. The tacn solution was added drop wise to the stirring $[Fe^{III}(DMF)_6](OTf)_3$ solution and stirred overnight. The solution was then filtered and placed in an ether chamber affording red-orange crystals after 24 h. Yield: 156 mg (58%) IR (KBr pellet, cm^{-1}): 3522 (w), 3249 (w), 3083 (m), 2855 (w), 2796 (w), 2315 (w), 1661 (s), 1483 (w), 1458 (w), 1434 (w), 1396 (w), 1252 (s), 1165 (s), 1111 (w), 1031 (m), 986 (w), 839 (w), 817 (w), 763 (w), 639 (m), 577 (w), 519 (w), 485 (w). UV-vis (CH_3OH) [λ_{max}, nm (ε, M^{-1} cm^{-1})]: 230 (22,000, sh), 281 (5,200, sh), 338 (356), 433 (105), 513 (45, sh). UV-vis (CH_3CN) [λ_{max}, nm (ε, M^{-1} cm^{-1})]: 252 (21,300), 333 (428), 432 (129), 513 (57, sh). UV-vis (DMF) [λ_{max}, nm (ε, M^{-1} cm^{-1})]: 340 (581), 432 (162), 520 (66, sh). Anal. Calcd for $C_{15}H_{30}F_9FeN_6O_9S_3$: C, 23.66; H, 3.97; N, 11.04. Found: C, 23.65; H, 3.98; N, 10.91.

Physical Measurements. ^1H NMR spectra were recorded at 25 °C on a Bruker Avance II 400 MHz instrument and sample peaks in [D]dichloromethane were referenced to TMS (tetramethylsilane). FT-IR spectra were measured on a Varian 3100 Excalibur Series. Optical spectra were collected on a Cary 50 UV-vis spectrophotometer. EPR spectra were recorded on a Bruker Model 300 ESP X-band spectrometer (9.37 GHz) at 77 K running WinEPR software. A 1 mM Cu complex[20] in DMF was used as a standard to calculate the spins in the $g \sim 2$ region while a 1 mM Fe^{III}-EDTA solution (prepared by stirring $FeCl_3 \cdot 6H_2O$ with excess

$Na_2EDTA{\cdot}2H_2O$ (Aldrich) for several hours) was used to calculate the spins in the g ~ 4.3 region. ESI-MS experiments were performed on a Thermo Finnigan TSQ Quantum Ultra AM triple quadrupole mass spectrometer.

X-Ray Crystallography. $[Fe^{III}(tacn)_2](OTf)_3$ (**3**) was crystallized by diffusion of ether in a methanol solution of **3**. An orange-red plate crystal with dimensions $0.53 \times 0.35 \times 0.15$ mm^3 was mounted on a Nylon loop using very small amount of paratone oil. Data were collected using a Bruker CCD (charge coupled device) based diffractometer equipped with an Oxford Cryostream low-temperature apparatus operating at 173 K. Data were measured using ω and ϕ scans of 0.5° per frame for 30 s. The total number of images was based on results from the program COSMO[21] where redundancy was expected to be 4.0 and completeness to 0.83 Å to 100%. Cell parameters were retrieved using APEX II software[22] and refined using SAINT on all observed reflections. Data reduction was performed using the SAINT software[23] which corrects for Lp. Scaling and absorption corrections were applied using SADABS[24] multi-scan technique, supplied by George Sheldrick. The structures are solved by the direct method using the SHELXS-97 program and refined by least squares method on F^2, SHELXL-97,[25] which are incorporated in OLEX2.[25] The structure was solved in the space group $P2_1/n$ (no. 14). All non-hydrogen atoms are refined anisotropically. Hydrogens were calculated by geometrical methods and refined as a riding model. Although there is disorder in one of the anions, $(SO_3CF_3)^-$, modeling of this disordered failed to yield chemical and crystallographic correct models and therefore no disorder model is provided here, although there is a large electron density peak within the anion. All drawings are done at 50% ellipsoids. Please Refer to Table 1 for additional crystal and refinement information. CCDC-1406004 contains the supplementary crystallographic

data for this paper. These data can be obtained free of charge from The Cambridge Crystallographic Data Centre via www.ccdc.cam.ac.uk/data_request/cif.

Magnetic Measurements. Variable temperature magnetic susceptibilities were measured using a Quantum Design MPMS SQUID magnetometer calibrated with a 765-Palladium standard purchased from NIST (formally NSB). Powdered samples were placed in plastic bags. Samples were measured in the temperature range 2–400 K (H = 0.1 T). The magnetic contribution of the bags were subtracted from the sample. Samples were placed in plastic straws for measurements. The molar magnetic susceptibilities were corrected for the diamagnetism of the complexes using tabulated values of Pascal's constants to obtain a corrected molar susceptibility. Solution magnetic susceptibility was determined using the Evan's Method (^{1}H NMR) at 298 K.[18] The mass susceptibility (χ_g) was calculated using Eq. 5:

$$\chi_g = \frac{-3\Delta f}{4\pi f m} + \chi_o\left[1 + \frac{(d_o - d_s)}{m}\right] \quad (5)$$

Where Δf is the frequency shift in Hz of the reference compound, f is the fixed probe frequency of spectrometer, χ_o is the mass susceptibility in 1 mL of solution, and d_o and d_s are the densities of the solvent and solution, respectively.

Computational details. Quantum chemical calculations providing energy minimized molecular geometries, molecular orbitals (HOMO-LUMO), and vibrational spectra for compound **2** and **3** were carried out using density functional theory (DFT) as implemented in the GAUSSIAN09 (Rev. C.01) program package.[26] We employed the hybrid functional PBE0[27] containing 25%

of exact exchange. We employed the basis set 6-31G(d).[28] Full ground state geometry optimization was carried out without any symmetry constraints. Only the default convergence criteria were used during the geometry optimizations. The initial geometry was taken from the crystal structure coordinates in the doublet state. Optimized structures were confirmed to be local minima (no imaginary frequencies for both cases). Molecular Orbitals were generated using Avogadro[29] (an open-source molecular builder and visualization tool, Version1.1.0. http://avogadro.openmolecules.net/).

Acknowledgements

Financial support from Oakland University (OU-REF) and NSF Grant No. CHE-0748607 is gratefully acknowledged. JL acknowledges a graduate fellowship from OU. The National Science Foundation (NSF) award (CHE-0821487) and National Institutes of Health (NIH) award (R15GM112395) are also acknowledged.

Keywords: Iron • Oxidation • EPR • DFT • Magnetic Properties

Supporting Information

Tables containing crystal data for **3** (21 pages).

[1] (a) E. A. Mader, E. R. Davidson and J. M. Mayer, *J. Am. Chem. Soc.* **2007**, *129*, 5153-5166; (b) E. A. Mader, V. W. Manner, T. F. Markle, A. Wu, J. A. Franz and J. M. Mayer, *J. Am. Chem. Soc.* **2009**, *131*, 4335-4345; (c) J. L. Li, S. D. Zhou, J. Zhang, M. Schlangen, T. Weiske, D. Usharani, S. Shaik and H. Schwarz, *J. Am. Chem. Soc.* **2016**, *138*, 7973-7981; (d) A. Pannwitz and O. S. Wenger, *Phys. Chem. Chem. Phys.* **2016**, *18*, 11374-11382; (e) J. L. Li, S. D. Zhou, X. N. Wu, S. Y. Tang, M. Schlangen and H. Schwarz, *Angew. Chem. Int. Ed.* **2015**, *54*, 11861-11864; (f) J. M. Mayer, *Acc. Chem. Res.* **2011**, *44*, 36-46.

[2] T. R. Porter and J. M. Mayer, *Chem. Sci.* **2014**, *5*, 372-380.

[3] (a) T. V. Chciuk, W. R. Anderson and R. A. Flowers, *J. Am. Chem. Soc.* **2016**, *138*, 8738-8741; (b) E. C. Gentry and R. R. Knowles, *Acc. Chem. Res.* **2016**, *49*, 1546-1556; (c) T. T. Eisenhart, W. C. Howland and J. L. Dempsey, *J. Phys. Chem. B* **2016**, *120*, 7896-7905; (d) H. G. Yayla, H. J. Wang, K. T. Tarantino, H. S. Orbe and R. R. Knowles, *J. Am. Chem. Soc.* **2016**, *138*, 10794-10797; (e) H. Mitome, T. Ishizuka, H. Kotani, Y. Shiota, K. Yoshizawa and T. Kojima, *J. Am. Chem. Soc.* **2016**, *138*, 9508-9520.

[4] (a) J. S. Kretchmer and T. F. Miller, *Inorg. Chem.* **2016**, *55*, 1022-1031; (b) H. M. Neu, R. A. Baglia and D. P. Goldberg, *Acc. Chem. Res.* **2015**, *48*, 2754-2764.

[5] A. V. Soudackov and S. Hammes-Schiffer, *J. Phys. Chem. Lett.* **2014**, *5*, 3274-3278.

[6] B. T. Saylor, L. A. Reinhardt, Z. B. Lu, M. S. Shukla, L. Nguyen, W. W. Cleland, A. Angerhofer, K. N. Allen and N. G. J. Richards, *Biochemistry* **2012**, *51*, 2911-2920.

[7] (a) T. Irebo, S. Y. Reece, M. Sjodin, D. G. Nocera and L. Hammarstrom, *J. Am. Chem. Soc.* **2007**, *129*, 15462-15464; (b) A. R. Offenbacher, L. A. Burns, C. D. Sherrill and B. A. Barry, *J. Phys. Chem. B* **2013**, *117*, 8457-8468; (c) D. J. Stewart, M. K. Brennaman, S.

E. Bettis, L. Wang, R. A. Binstead, J. M. Papanikolas and T. J. Meyer, *J. Phys. Chem. Lett.* **2011**, *2*, 1844-1848.

[8] M. R. A. Blomberg and P. E. M. Siegbahn, *Biochim. Biophys. Acta* **2006**, *1757*, 969-980.

[9] (a) H. Hirao and P. Chuanprasit, *Chem. Phys. Lett.* **2015**, *621*, 188-192; (b) Y. Wang, H. Hirao, H. Chen, H. Onaka, S. Nagano and S. Shaik, *J. Am. Chem. Soc.* **2008**, *130*, 7170-7171.

[10] (a) D. Wang and L. Que, *Chem. Commun.* **2013**, *49*, 10682-10684; (b) M. Merkx, D. A. Kopp, M. H. Sazinsky, J. L. Blazyk, J. Muller and S. J. Lippard, *Angew. Chem. Int. Ed.* **2001**, *40*, 2782-2807.

[11] L. Olshansky, B. L. Greene, C. Finkbeiner, J. Stubbe and D. G. Nocera, *Biochemistry* **2016**, *55*, 3234-3240.

[12] J. P. Roth, J. C. Yoder, T. J. Won and J. M. Mayer, *Science* **2001**, *294*, 2524-2526.

[13] A. S. Tolla, A. Banerjee, S. Stjepanovic, J. Li, W. W. Brennessel, R. Loloee and F. A. Chavez, *Eur. J. Inorg. Chem.* **2013**, 2115–2121.

[14] (a) A. Jordan and B. Steinberg, *Atmos. Meas. Tech.* **2011**, *4*, 509-521; (b) T. Kawano, N. Tsuboi, H. Tsujii, T. Sugiyama, Y. Asakura, T. Uda, *J. Chromatogr. A* **2004**, *1023*, 123-127.

[15] K. Wieghardt, W. Schmidt and W. Herrmann, *Inorg. Chem.* **1983**, *22*, 2953–2956.

[16] (a) T. Fujinami, K. Nishi, R. Kitashima, K. Murakami, N. Matsumoto, S. Iijima and K. Toriumi, *Inorg. Chim. Acta* **2011**, *376*, 136-143; (b) D. J. Harding, D. Sertphon, P. Harding, K. S. Murray, B. Moubaraki, J. D. Cashion and H. Adams, *Chem. Eur. J.* **2013**, *19*, 1082-1090; (c) M. Koike, K. Murakami, T. Fujinami, K. Nishi, N. Matsumoto and Y. Sunatsuki, *Inorg. Chim. Acta* **2013**, *399*, 185-192; (d) M. Martinho, G. Q. Xue, A. T.

Fiedler, L. Que, E. L. Bominaar and E. Munck, *J. Am. Chem. Soc.* **2009**, *131*, 5823-5830; (e) D. Sertphon, D. J. Harding, P. Harding, K. S. Murray, B. Moubaraki, J. D. Cashion and H. Adams, *Eur. J. Inorg. Chem.* **2013**, 788-795; (f) C. F. Sheu, S. M. Chen, G. H. Lee, Y. H. Liu, Y. S. Wen, J. J. Lee, Y. C. Chuang and Y. Wang, *Eur. J. Inorg. Chem.* **2013**, 894-901; (g) A. Tissot, P. Fertey, R. Guillot, V. Briois and M. L. Boillot, *Eur. J. Inorg. Chem.* **2014**, 101-109; (h) J. C. A. Boeyens, A. G. S. Forbes, R. D. Hancock and K. Wieghardt, *Inorg. Chem.* **1985**, *24*, 2926–2931.

[17] K. Pohl, K. Wieghardt, W. Kaim and S. Steenken, *Inorg. Chem.* **1988**, *27*, 440-447.

[18] C. Piguet, *J. Chem. Ed.* **1997**, *74*, 815-816.

[19] G. H. Searle and R. J. Geue, *Aust. J. Chem.* **1984**, *37*, 959–970.

[20] A. Y. S. Malkhasian, M. E. Finch, B. Nikolovski, A. Menon, B. E. Kucera and F. A. Chavez, *Inorg. Chem.* **2007**, *46*, 2950-2952.

[21] *COSMO V1.61, Software for the CCD Detector Systems for Determining Data Collection Parameters. Bruker Analytical X-ray Systems, Madison, WI (2009).*

[22] *APEX2 V2010.11-3. Software for the CCD Detector System; Bruker Analytical X-ray Systems, Madison, WI (2010).*

[23] *SAINT V 7.68A Software for the Integration of CCD Detector System Bruker Analytical X-ray Systems, Madison, WI (2010).*

[24] *SADABS V2008/2 Program for absorption corrections using Bruker-AXS CCD based on the method of Robert Blessing;* Blessing, R.H., *Acta Cryst.* **1995**, *A51*, 33-38.

[25] Sheldrick, G.M. *"A short history of SHELX". Acta Cryst.* **2008**, *A64*, 112-122.

[26] M. J. Frisch, *et al. Gaussian09, Revision C.01, Gaussian Inc., Wallingford CT, 2010*.

[27] C. Adamo and V. Barone, *J. Chem. Phys.* **1999**, *110*, 6158–6170.

[28] G. A. Petersson and M. A. Al-Laham, *J. Chem. Phys.* **1991**, *94*, 6081–6090.

[29] M. Hanwell, D. Curtis, D. Lonie, T. Vandermeersch, E. Zurek and G. Hutchison, *J. Cheminf.* **2012**, *4*, 1-17.

We report a thermally initiated proton-coupled electron transfer (PCET) reaction for $[Fe^{II}(tacn)_2](OTf)_2$ (**1**). Compound **1** undergoes slow oxidation when heated under dynamic vacuum by loss of an H atom yielding a deprotonated tacn ligand (tacn-H) and H_2. Formation of $[Fe^{III}(tacn)(tacn\text{-}H)](OTf)_2$ (**2**) from **1** was confirmed by ESI-MS. Synthesis of **2** was carried out by reacting structurally characterized $[Fe^{III}(tacn)_2](OTf)_3$ with one equiv base.

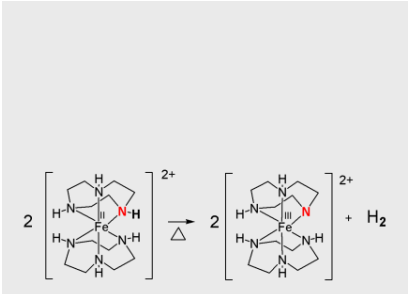

Thermally Induced PCET

*Jia Li, Atanu Banerjee, Debra R. Preston, Brian J. Shay, Amitiva Adhikary, Michael D. Sevilla, Reza Loloee, Richard J. Staples, Ferman A. Chavez**

Page No. – Page No.

Thermally Induced Oxidation of $[Fe^{II}(tacn)_2](OTf)_2$ (tacn = 1,4,7-triazacyclononane)